

## Causes and elimination of pyramidal defects in GaSb-based epitaxial layers

Lee M. Murray, Asli Yildirim, Sydney R. Provence, Dennis T. Norton, Thomas F. Boggess et al.

Citation: *J. Vac. Sci. Technol. B* 31, 03C108 (2013); doi: 10.1116/1.4792515

View online: <http://dx.doi.org/10.1116/1.4792515>

View Table of Contents: <http://avspublications.org/resource/1/JVTBD9/v31/i3>

Published by the AVS: Science & Technology of Materials, Interfaces, and Processing

---

### Additional information on J. Vac. Sci. Technol. B

Journal Homepage: <http://avspublications.org/jvstb>

Journal Information: [http://avspublications.org/jvstb/about/about\\_the\\_journal](http://avspublications.org/jvstb/about/about_the_journal)

Top downloads: [http://avspublications.org/jvstb/top\\_20\\_most\\_downloaded](http://avspublications.org/jvstb/top_20_most_downloaded)

Information for Authors: [http://avspublications.org/jvstb/authors/information\\_for\\_contributors](http://avspublications.org/jvstb/authors/information_for_contributors)

### ADVERTISEMENT



AMERICAN  
ELEMENTS

**Now Invent.<sup>TM</sup>**

The World's Manufacturer  
of Engineered &  
Advanced Materials

[www.americanelements.com](http://www.americanelements.com)

# Causes and elimination of pyramidal defects in GaSb-based epitaxial layers

Lee M. Murray,<sup>a)</sup> Asli Yildirim, Sydney R. Provence, and Dennis T. Norton

*Department of Physics and Astronomy and Optical Science and Technology Center, University of Iowa, Iowa City, Iowa 52242*

Thomas F. Boggess and John P. Prineas

*Department of Physics and Astronomy, Optical Science and Technology Center, and Department of Electrical and Computer Engineering, University of Iowa, Iowa City, Iowa 52242*

(Received 21 November 2012; accepted 4 February 2013; published 20 February 2013)

Here, the authors report on the occurrence, cause, and elimination of pyramidal defects in layers of GaSb grown by molecular beam epitaxy on GaSb substrates. These defects are typically 3–8 nm high, 1–3 μm in diameter, and shaped like pyramids. Their occurrence in the growth of GaSb buffer layers can propagate into subsequent layers such as GaSb, GaInAsSb, and GaSb/InAs superlattices. Defects are nucleated during the early stages of growth after the thermal desorption of native oxide from the GaSb substrate. These defects grow into pyramids due to a repulsive Ehrlich–Schwoebel potential on atomic step edges leading to an upward adatom current. The defects reduce in density with growth of GaSb. The insertion of a thin AlAsSb layer into the early stages of the GaSb buffer increases the rate of elimination of the defects, resulting in a smooth surface within 500 nm. The acceleration of defect reduction is due to the temporary interruption of step-flow growth induced by the AlAsSb layer. This leads to a reduced isolation of the pyramids from the GaSb epitaxial layer and allows the pyramidal defects to smooth out. © 2013 American Vacuum Society.

[<http://dx.doi.org/10.1116/1.4792515>]

## I. INTRODUCTION

The 6.1 Å III–V compound semiconductors, including InAs, GaSb, AlSb, and their alloys, grown lattice-matched to GaSb substrates are an important family of materials for infrared optoelectronic devices,<sup>1</sup> including lasers,<sup>2–4</sup> light-emitting diodes,<sup>3–5</sup> photodiode detectors,<sup>6–12</sup> and thermophotovoltaics.<sup>13</sup> Epitaxial growth of high-quality material requires minimizing surface defect densities to minimize nonradiative recombination rates and maximize device yield from the wafer. High quality layers begin with growth of smooth buffer layers free of defects, which can otherwise propagate into subsequent epitaxial heterostructure layers. Additionally, a rougher starting surface has been associated with increased decomposition of metastable layers.<sup>14</sup>

Smooth GaSb buffer layers on GaSb substrates have been reported in metal-organic chemical vapor deposition (MOCVD) layers by first chemically thinning the substrate oxide layer prior to growth, even for “epi-ready” substrates; otherwise, the thick oxide consumes Ga from the substrate during desorption, resulting in pitting of the surface.<sup>15</sup> However, there are a lack of studies of the morphology of GaSb buffer layers grown by molecular beam epitaxy (MBE). There is also a perception that growth of GaSb-based semiconductors may be better suited to MBE than MOCVD due to greater accessibility to growth at lower temperatures, lack of complications introduced by precursors, and other factors.<sup>16–19</sup> Studies that do exist have reported high densities of mesoscopic defects, often pyramidal in shape,<sup>20,21</sup> at typical densities of  $10^4$  to  $10^5 \text{ cm}^{-2}$ .<sup>22</sup> The typical approach to minimizing their formation, with limited success, has focused on optimizing the deoxidation procedure.

<sup>a)</sup>Electronic mail: lee-murray@uiowa.edu

The formation of pyramidal defects in MBE systems has been studied theoretically and experimentally in the past.<sup>23–30</sup> These studies suggest that the formation of pyramidal defects is a result of morphological instability. Instability during growth can lead to the formation of small islands on the surface. The presence of an Ehrlich–Schwoebel barrier, which acts as a resistive force to adatoms trying to move down atomic steps, results in an upward adatom current on the island leading to the formation of a pyramid, Fig. 1. It is possible to reduce the degree of instability by either altering growth conditions or switching to vicinal substrates. While the Ehrlich–Schwoebel barrier can work as a generation mechanism for the pyramids, it also has a stabilizing effect on vicinal surfaces, as shown schematically in Fig. 2.

We have recently observed the formation of pyramidal defects in GaSb buffer layers grown using molecular beam epitaxy and found an effective method of removing them by

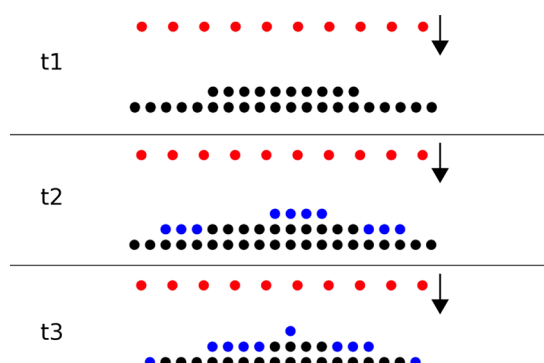


FIG. 1. (Color online) Ehrlich–Schwoebel barrier has a destabilizing effect on islands. Here, the adatom step barrier promotes the growth of pyramidal structures on the surface.

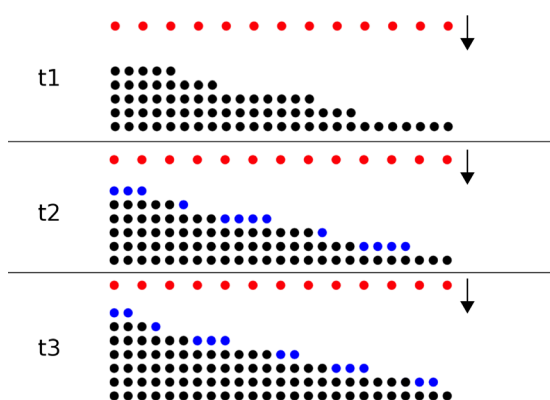


FIG. 2. (Color online) Ehrlich–Schwoebel barrier can act as a stabilizing force during epitaxial growth on stepped surfaces. The steps that are wider (narrower) than normal receive more (less) adatoms. This promotes uniform step sizes in the long term.

insertion of a thin layer of AlAsSb in the GaSb buffer layer. What follows is an investigation of the causes of pyramidal defects and why a thin layer of AlAsSb removes them. Such defects are linked to the removal of native oxide prior to epitaxial growth.

## II. EXPERIMENT

All samples were grown in a Veeco Gen20 MBE system with valved arsenic and antimony crackers. Wafers were etched in hydrochloric acid and rinsed with isopropanol prior to being diced into quarters and loaded into the system.<sup>15,31</sup> Wafers were outgassed in a separate chamber for 1 h at 225 °C prior to introduction to the growth chamber. Samples were deoxidized prior to growth under an Sb overpressure to remove residual oxide in an optimized procedure described elsewhere.<sup>22</sup> The oxide removal was observed with reflection high-energy electron diffraction (RHEED) and occurred at ~515 °C. Substrates were annealed for 15 min at ~525 °C to ensure complete oxide removal. Temperatures were monitored using a BandiT temperature monitoring system operating in blackbody mode. This was calibrated using the 1 × 3 to 1 × 5 RHEED transition of GaSb.<sup>32</sup>

GaSb buffer layers were grown using a true V/III flux ratio of ~1.3.<sup>33</sup> All growths were done with a GaSb growth rate of 0.6 ml/s and a substrate temperature of 500 °C. AlAsSb layers were also grown at 0.6 ml/s and 500 °C. Separate growths and high-resolution x-ray diffraction were used to verify lattice matching of the AlAsSb layers.

Upon initial observation of pyramidal defects, attempts were made to remove them through modification of desorption and growth parameters. Changes in the level of antimony flux, anneal temperatures, and anneal times during desorption failed to remove the observed defects. Changes in V/III ratios and growth temperature also failed to remove the defects.

Surface investigations were undertaken using atomic force microscopy (AFM) under atmosphere. All samples were scanned over 90 × 90  $\mu\text{m}^2$  and 20 × 20  $\mu\text{m}^2$  areas. Some samples had additional scans with smaller areas. All AFM data analysis and plotting was done using the GWYDION software package.

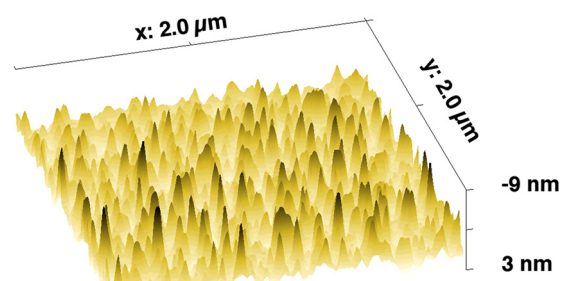


FIG. 3. (Color online) AFM image of GaSb wafer after oxide removal. The vertical axis is inverted so the pits appear as peaks. This pitting is due to the  $\text{Sb}_2\text{O}_3$  reacting with the GaSb surface.

## III. RESULTS AND DISCUSSION

Thermal desorption of oxide from a GaSb wafer causes damage to the wafer. This damage is visible in AFM scans as pitting of the surface (Fig. 3). The roughness is rounded and does not show any ordered pyramidal shape. However,

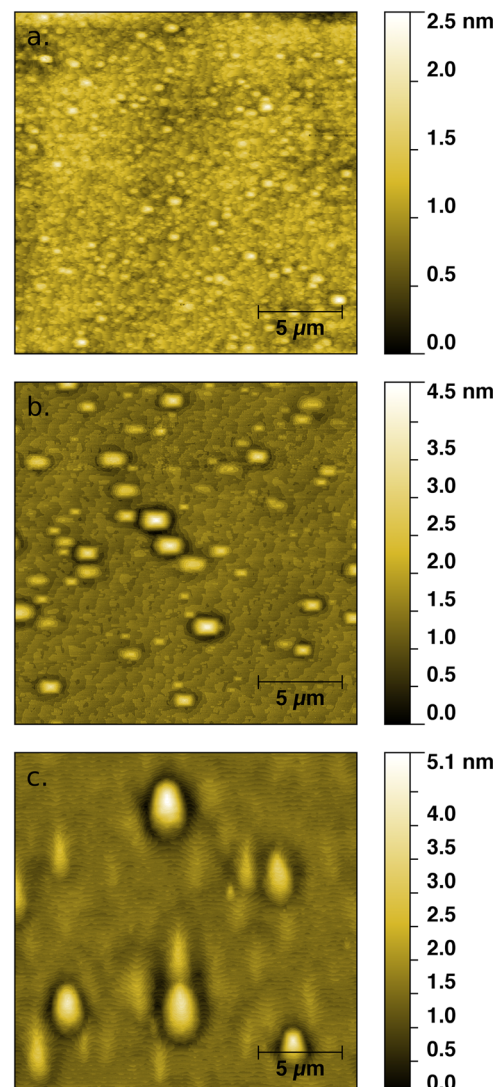


FIG. 4. (Color online) AFM images of GaSb surfaces with no AlAsSb layers at three thicknesses: (a) 30 nm, (b) 200 nm, and (c) 650 nm. Defects grow in size, both laterally and vertically, but decrease in density as layer thickness increases.

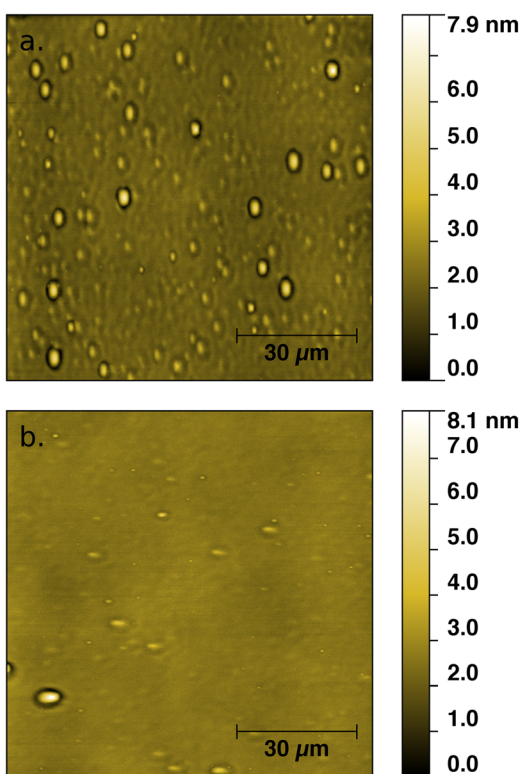


FIG. 5. (Color online) AFM image of (a) 1  $\mu\text{m}$  and (b) 2  $\mu\text{m}$  GaSb layers. By the time, 2  $\mu\text{m}$  of material has been grown and the density of defects has dropped considerably.

after only 30 nm of growth of GaSb, the pyramidal defects are visible (Fig. 4). The defects remain present at high densities for growth thicknesses up to 650 nm (Fig. 4). As further GaSb is grown, the density of defects decreases. This self-smoothing effect would likely lead to an almost defect-free surface eventually but is not a feasible solution to defects in GaSb buffer layers as there are still appreciable defect densities after 2  $\mu\text{m}$  of GaSb homoepitaxy (Fig. 5). As the thickness of GaSb increases, pyramidal defects are observed to grow both laterally and vertically. It is also clear that the defects are isolated from the underlying surface. They exist as islands, with a complete ring of material isolating them from the wafer they are grown upon (Fig. 6).

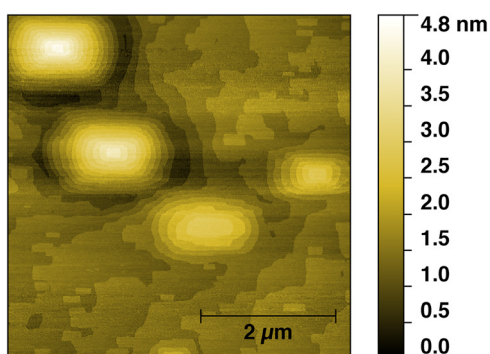


FIG. 6. (Color online) AFM image of 200 nm GaSb with no AlAsSb layer. Notice the clearly defined pyramidal structure of the defects as well as the isolation of the layer structure of the defects from the step flow pattern of the underlying epilayer.

The efficient elimination of these defects was discovered by reverse engineering samples with good surfaces. We had found that thick GaSb photoluminescence samples clad with thin AlAsSb confinement layers—grown to check material quality and not as part of the investigation into these defects—had no pyramidal defects. We then proceeded to remove the top confinement layer, and thin the GaSb emission layer down, checking for defects at each step, which we found no evidence of. This resulted in the discovery that a thin layer of lattice matched AlAsSb inserted into a GaSb buffer layer dramatically and efficiently removed the pyramidal defects. Compare for example Figs. 4(c) and 7.

Next, we investigated what caused the formation of the pyramidal defects and why the thin AlAsSb layer inserted into the GaSb buffer layer eliminated them. The defects are generated as a result of growth on the roughened substrate surface after deoxidation. To investigate the effect of oxide removal on defect formation, two samples were regrown on. Both samples consisted of 150 nm of GaSb, 30 nm of AlAsSb, and then 500 nm of additional GaSb, which as shown in Fig. 7 results in a defect-free surface with visible step-flow growth. After growth of these two structures, one was removed from vacuum and allowed to sit for several months in atmosphere, allowing a thick oxide layer to develop. The other was never removed from vacuum but was put through the same outgas preheat as all other growths. Both samples were then put through the same desorption recipe and had 200 nm of GaSb deposited on their surface. A comparison of the two samples is shown in Fig. 8. The sample that had been exposed to atmosphere developed a clear pattern of pyramidal defects, while the sample with no oxide prior to desorption had no sign of pyramidal defects. Desorption of GaSb is known to damage the underlying surface, causing pitting of the wafer surface as shown in Fig. 3.<sup>14</sup> This damage may cause the pyramidal defects to form, although the exact mechanism that leads to their nucleation is not well understood. Pyramidal defects in GaSb due to a roughened starting surface following wafer deoxidation have been observed by others.<sup>20</sup>

Our own previous investigations into optimum GaSb buffer growth<sup>22</sup> did not reveal pyramidal defects. The previous study was performed in a different MBE chamber, an

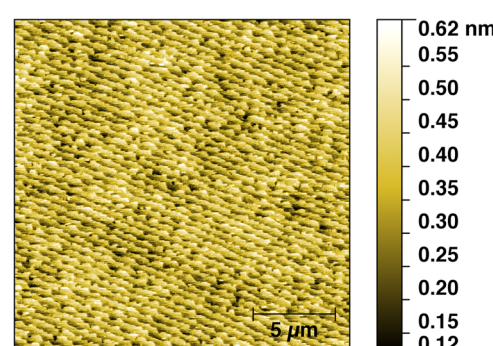


FIG. 7. (Color online) AFM image of buffer layer consisting of 150 nm GaSb, 30 nm AlAsSb, and 500 nm of GaSb. Vertical scale is truncated to emphasize good step-flow pattern; full scale is 0–0.79 nm.

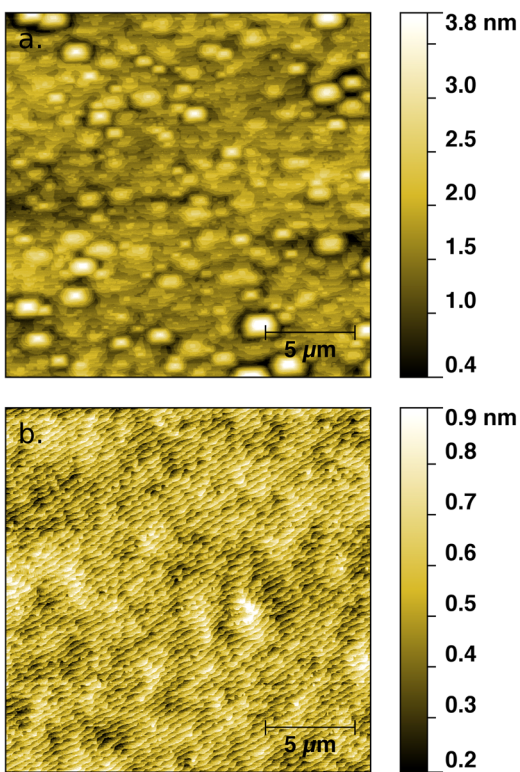


FIG. 8. (Color online) AFM images of regrown GaSb surfaces. Both images are 200 nm of GaSb grown on a previously grown wafer consisting of 150 nm GaSb, 30 nm AlAsSb, and 500 nm GaSb. In (a), the wafer was allowed to develop an oxide layer in between the first and second growths; in (b), the sample was kept under vacuum to prevent an oxide layer from forming. Vertical scales are truncated to show fine detail. Full scale for each is 5.2 and 1.24 nm, respectively.

EPI930, than the current study, which used a newly installed Gen20. Because identical deoxidation and growth conditions were used in GaSb growth, we were concerned that a contaminant in the chamber may be contributing to the nucleation of these defects. A combination of mass spectrometer scans of the chamber and secondary ion mass spectrometry scans of samples showed no evidence of excess chamber contaminants or incorporation into epilayers relative to the EPI 930 system. We have performed growths in the EPI930 and can now see evidence of the pyramidal defects; however, the density is lower than in epilayers grown in the Gen20 system. We speculate that differences between the systems result in different levels of postdesorption surface roughness, which lead to different pyramidal defect densities. While it is clear that the defects nucleate on the roughened surface created during oxide removal, the exact nucleation method is not understood in detail.

While the exact nucleation mechanism is not clear, we can rule out the standard explanation of pyramidal defects arising due to growth instability. The cause of the pyramidal defects observed here is clearly transitory. This can be seen both from the self smoothing behavior observed with increasing GaSb thickness and by the fact that the defects do not return once removed, as seen in Fig. 9.

The AlAsSb layer does not immediately remove the defects; defects are readily visible in the early layers of

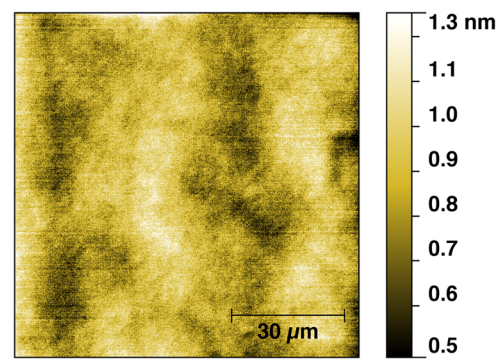


FIG. 9. (Color online) AFM image of surface of 2000 nm of GaSb grown on 150 nm of GaSb and 30 nm of AlAsSb. The surface is nearly defect-free and shows visible step flow growth. The vertical scale has been truncated. Full scale is 1.6 nm.

growth of GaSb on top of the AlAsSb. Imaging the AlAsSb layer directly shows a breakdown of step-flow growth, Fig. 10. Further evidence of a reduction in step flow growth is visible in RHEED oscillations, Fig. 11. The RHEED oscillations of GaSb show strong damping of both the minimum and maximum intensities. This is evidence of a mixing of step-flow and island growth modes.<sup>34</sup> The oscillations for AlAsSb show less damping of the minimum value, indicating a less pronounced step flow character. After GaSb growth is resumed, step flow returns. However, the pyramidal defects are less isolated now than before. This can be seen by comparing the defects in Fig. 12 with those in Fig. 6. This reduction in isolation disrupts the adatom diffusion currents up the pyramid sidewalls, which then allows the pyramidal defects to be eliminated by additional GaSb growth. A nearly defect-free surface evolves in just 500 nm of growth on top of AlAsSb. This surface remains defect-free with the deposition of additional GaSb—up to 2  $\mu$ m has been imaged—as in Fig. 9.

The removal of defects after deposition of AlAsSb seems to be the same mechanism as the self-smoothing observed with increasing thickness of GaSb. Images of the 650 nm and 1  $\mu$ m thick GaSb samples without AlAsSb show a similar reduction in isolation and a reduction in the pyramidal symmetry of the defects, Fig. 13. However, the reduction in

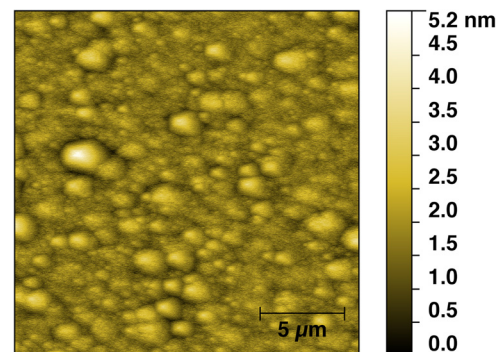


FIG. 10. (Color online) AFM images of 30 nm of AlAsSb on top of 150 nm of GaSb. There is no sign of step-flow visible in the AlAsSb; the defect density is also elevated compared to growth of just GaSb.

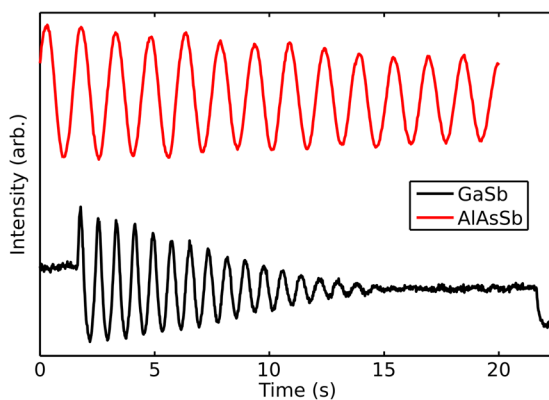


FIG. 11. (Color online) RHEED oscillations during growth of GaSb and AlAsSb layers. Curves have been offset for clarity. The reduced damping of the minima in the AlAsSb RHEED curve indicates a reduced amount of step progression during growth of that material.

defect isolation due to the insertion of the AlAsSb layer accelerates this smoothing process dramatically.

#### IV. SUMMARY AND CONCLUSIONS

In this study, we investigated the formation of pyramidal defects in GaSb buffer layers grown on GaSb substrates. These defects nucleated on the roughened, deoxidized substrate surface. While GaSb homoepitaxy undergoes self-smoothing, the mechanism is slow and requires very thick

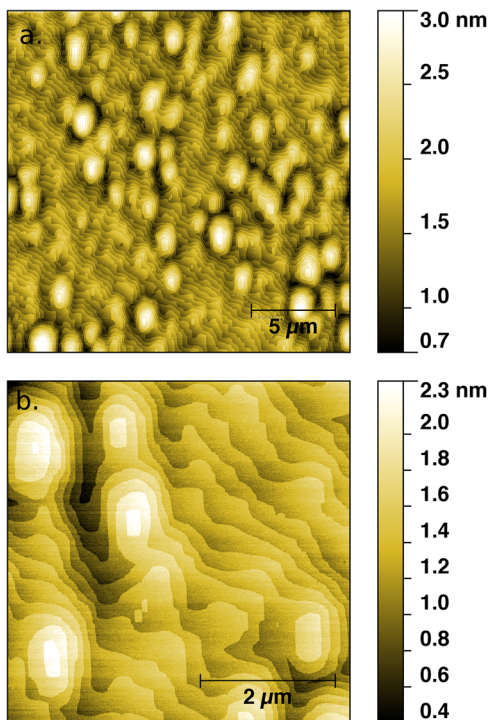


FIG. 12. (Color online) AFM image of 20 nm of GaSb grown on top of 150 nm of GaSb and 30 nm of AlAsSb. Step-flow growth has returned, though the defect density is still elevated compared to pure GaSb growth. However, the pyramids are significantly less isolated. This reduction in isolation speeds the smoothing of the surface, as can be seen in the 5 by 5  $\mu\text{m}^2$  image (b). The step-flow pattern bends around the defects but is not isolated from them as it was prior to the insertion of the AlAsSb. Vertical scales are truncated to show detail; full scale is 3.9 nm for (a) and 2.7 nm for (b).

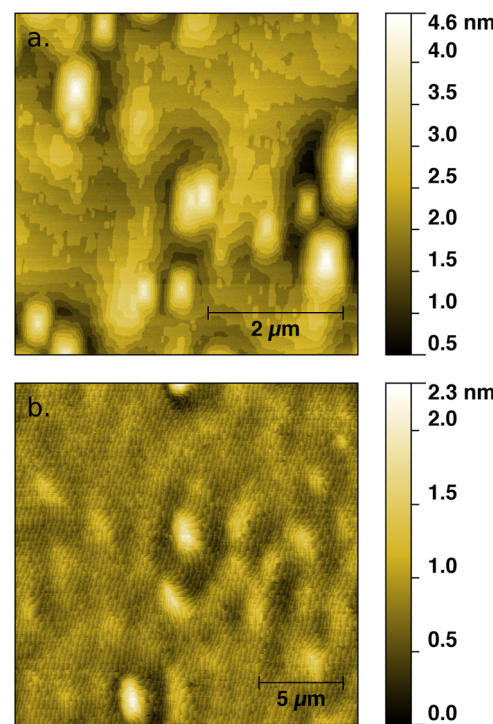


FIG. 13. (Color online) Reduction in isolation of defects as the GaSb thickness increases. At 650 nm of GaSb with no AlAsSb layer, there is evidence of some reduction in isolation between pyramids and surface (a). By the time 1  $\mu\text{m}$  has been grown, there is a significant reduction in the pyramidal nature of the defects (b).

buffer layers. Insertion of a lattice matched AlAsSb ternary layer temporarily interrupts step-flow growth. This interruption removes the isolation of the pyramidal defects from the rest of the growth surface, enhancing the rate at which the surface smooths. The buffer design of 150 nm GaSb, 30 nm AlAsSb, and 500 nm GaSb provides a pyramidal defect-free surface for the growth of antimonide-based heterostructures.

#### ACKNOWLEDGMENTS

The authors would like to thank the NSF for funding under DRM 100-6956. The authors would also like to acknowledge the staff of the Central Microscopy Research Facility (CMRF). All AFM images were generated at the CMRF.

- <sup>1</sup>P. S. Dutta, H. L. Bhat, and V. Kumar, *J. Appl. Phys.* **81**, 5821 (1997).
- <sup>2</sup>D. Z. Garbusov, H. Lee, V. Khalfin, R. Martinelli, J. C. Connolly, and G. L. Belenky, *IEEE Photon. Technol. Lett.* **11**, 794 (1999).
- <sup>3</sup>C. Lin, M. Grau, O. Dier, and M. C. Amann, *Appl. Phys. Lett.* **84**, 5088 (2004).
- <sup>4</sup>R. Liang, J. Chen, G. Kipshidze, D. Westerfeld, L. Shterengas, and G. Belenky, *IEEE Photon. Technol. Lett.* **23**, 603 (2011).
- <sup>5</sup>T. N. Danilova, B. E. Zhurtnov, A. N. Imenkov, and Y. P. Yakovlev, *Semiconductors* **39**, 1235 (2005).
- <sup>6</sup>J. P. Prineas, J. T. Olesberg, J. R. Yager, C. Cao, C. Coretsopoulos, and M. H. M. Reddy, *Appl. Phys. Lett.* **89**, 211108 (2006).
- <sup>7</sup>E. J. Koerperick, J. T. Olesberg, T. F. Boggess, J. L. Hicks, L. S. Wassink, L. M. Murray, and J. P. Prineas, *Appl. Phys. Lett.* **92**, 121106 (2008).
- <sup>8</sup>M. H. M. Reddy, J. T. Olesberg, C. Cao, and J. P. Prineas, *Semicond. Sci. Technol.* **21**, 267 (2006).
- <sup>9</sup>H. Shao, A. Torfi, W. Li, D. Moscicka, and W. I. Wang, *J. Cryst. Growth* **311**, 1893 (2009).

- <sup>10</sup>D. L. Smith and C. Mailhiot, *J. Appl. Phys.* **62**, 2545 (1987).
- <sup>11</sup>F. Fuchs, U. Weimer, W. Pletschen, J. Schmitz, E. Ahlsweide, M. Walther, J. Wagner, and P. Koidl, *Appl. Phys. Lett.* **71**, 3251 (1997).
- <sup>12</sup>D. Z. Y. Ting, C. J. Hill, A. Soibel, S. A. Keo, J. M. Mumolo, J. Nguyen, and S. D. Gunapala, *Appl. Phys. Lett.* **95**, 023508 (2009).
- <sup>13</sup>C. A. Wang, H. K. Choi, S. L. Ransom, G. W. Charache, L. R. Danielson, and D. M. Depoy, *Appl. Phys. Lett.* **75**, 1305 (1999).
- <sup>14</sup>C. A. Wang, D. A. Shiao, and A. Lin, *J. Cryst. Growth* **261**, 385 (2004).
- <sup>15</sup>C. J. Vineis, C. A. Wang, and K. F. Jensen, *J. Cryst. Growth* **225**, 420 (2001).
- <sup>16</sup>A. Aardvark, N. J. Mason, and P. J. Walker, *Prog. Cryst. Growth Charact.* **35**, 207 (1997).
- <sup>17</sup>C. A. Wang, S. Salim, K. F. Jensen, and A. C. Jones, *J. Cryst. Growth* **170**, 55 (1997).
- <sup>18</sup>Y. Huang, J. H. Ryou, R. D. Dupuis, A. Petschke, M. Mandl, and S. L. Chuang, *Appl. Phys. Lett.* **96**, 251107 (2010).
- <sup>19</sup>C. A. Wang, *J. Cryst. Growth* **272**, 664 (2004).
- <sup>20</sup>B. Z. Nosho, B. R. Bennett, E. H. Aifer, and M. Goldenberg, *J. Cryst. Growth* **236**, 155 (2002).
- <sup>21</sup>E. H. Aifer, E. M. Jackson, B. R. Bennett, I. Vurgaftman, J. R. Meyer, and G. G. Jernigan, Mater. Res. Soc. Symp. Proc. **722** (2002).
- <sup>22</sup>E. J. Koerperick, L. M. Murray, D. T. Norton, T. F. Boggess, and J. P. Prieneas, *J. Cryst. Growth* **312**, 185 (2010).
- <sup>23</sup>C. Orme, M. D. Johnson, K.-T. Leung, B. G. Orr, P. Smilauer, and D. Vvedensky, *J. Cryst. Growth* **150**, 128 (1995).
- <sup>24</sup>A. W. Hunt, C. Orme, D. R. M. Williams, B. G. Orr, and L. M. Sander, *Europhys. Lett.* **27**, 611 (1994).
- <sup>25</sup>M. D. Johnson, C. Orme, A. W. Hunt, D. Graff, J. Sudijono, L. M. Sander, and B. G. Orr, *Phys. Rev. Lett.* **72**, 116 (1994).
- <sup>26</sup>G. S. Bales and A. Zangwill, *Phys. Rev. B* **41**, 5500 (1990).
- <sup>27</sup>M. A. Herman and T. G. Andersson, *Appl. Phys. A* **41**, 243 (1986).
- <sup>28</sup>O. Pierre-Louis, M. R. D'Orsogna, and T. L. Einstein, *Phys. Rev. Lett.* **82**, 3661 (1999).
- <sup>29</sup>S. Schinzer, M. Kinne, M. Biehl, and W. Kinzel, *Surf. Sci.* **439**, 191 (1999).
- <sup>30</sup>P. Smilauer, *Vacuum* **50**, 115 (1998).
- <sup>31</sup>Z. Y. Liu, B. Hawkins, and T. F. Keuch, *J. Vac. Sci. Technol. B* **21**, 71 (2003).
- <sup>32</sup>A. S. Bracker, M. J. Yang, B. R. Bennett, J. C. Culbertson, and W. J. Moore, *J. Cryst. Growth* **220**, 384 (2000).
- <sup>33</sup>True V/III flux ratio refers to the V/III beam equivalent pressure (BEP) ratio divided by the V/III BEP ratio observed for stoichiometric growth.
- <sup>34</sup>P. I. Cohen, G. S. Petrich, and G. J. Whaley, in *Molecular Beam Epitaxy: Applications to Key Materials*, edited by R. F. C. Farrow (Noyes, Park Ridge, 1995), Chap. 8.